Available online at www.sciencedirect.com
ScienceDirect
Microporous and Mesoporous Materials 115 (2008) 113–122
MICROPOROUS AND MESOPOROUS MATERIALS
www.elsevier.com/locate/micromeso

ZSM5 growth on a FeCrAl steel support. Coating characteristics upon the catalytic behavior in the NO_x SCR

Juan M. Zamaro *, María A. Ulla, Eduardo E. Miró

Instituto de Investigaciones en Catálisis y Petroquímica, INCAPE (FIQ, UNL CONICET), Santiago del Estero 2829, 3000 Santa Fe, Argentina

Received 27 July 2007; accepted 6 November 2007
Available online 19 February 2008

Abstract

The search for more efficient catalytic processes requires the development of new structured catalytic systems. Along these lines, a study was conducted to produce and characterize a structured catalyst composed of an ordered ZSM5 catalytic coating onto an FeCrAl alloy steel support. The film obtained by secondary hydrothermal synthesis without templates was studied by SEM, EPMA, and XRD; then, it was catalytically tested for the SCR of NO_x with CH_4.

The growths were polycrystalline, dense, continuous and fast produced with a noticeable *c*-axis orientation perpendicular to the support surface. The FeCrAl surface made it possible to produce an adherent, Cr, Al, Fe-enriched coating.

The indium-exchanged system had a good performance in the SCR of NO_x with CH_4 although the NO_x to N_2 conversion was somehow lower than for the powder catalyst. This could be due to a lower accessibility of the active sites given the unfavorable orientation of the zeolitic channels. On the contrary, the catalyst behavior was better in terms of selectivity to N_2 and CO emission, probably due to both the low amount of non-selective indium species and the presence of oxidizing Fe species.

The results obtained with this system indicate the importance of considering the crystalline spatial position of the coating and the chemical influence of the support in the search for the optimized performance of a structured catalyst.

Keywords: ZSM5 coating; Metallic monolith; Oriented zeolite growth; NO_x SCR catalyst; Secondary ZSM5 growth

1. Introduction

Film zeolites for catalytic purposes have developed widely over the last decade. The applications in which these structured systems are mostly employed are those involving the treatment of high fluid flows and/or severe thermomechanical conditions in which the use of fixed-bed reactors is not advisable [1]. There are different types of supports and zeolites employed to produce these catalysts while washcoating and hydrothermal synthesis growth are the most usual coating methods [2]. Even though a more porous coating can be relatively simply obtained by washcoating, the growth method yields dense, mechanically stable growths while preventing the use of agglomerants to improve adherence. Two hydrothermal zeolite growth alternatives are available: direct or secondary synthesis. The latter can reduce the difficulties in the nucleation process onto the support surface [3]. Secondary growths usually present a crystallographic orientation and various studies focusing on this aspect, mainly for MFI membranes, can be found in the literature [4,5]. For those zeolite membranes, some variables such as seed concentration and seed size lead to different film microstructures and orientations. This phenomenon has no generalized explanation for all zeolite growths on supports of different nature although for MFI the competitive growth process [6] is the accepted mechanism and it has been simulated on flat surfaces [7,8]. MFI secondary growths can also be constituted by intergrowth crystals with either *a*-, *b*-, or *c*-axes perpendicular to the support. Other orientations can also be found, e.g. oblique orientations [8].

* Corresponding author.
E-mail addresses: emiro@fiqus.unl.edu.ar, zamaro@fiqus.unl.edu.ar (J.M. Zamaro).

1387-1811/$ - see front matter © 2008 Elsevier Inc. All rights reserved.
doi:10.1016/j.micromeso.2007.11.048

Most of the studies cited above on MFI secondary growths were performed for separation and pervaporation processes, while only a few were carried out for catalytic purposes [9]. Moreover, most MFI growth studies have focused on silicalites, which are not useful for catalytic applications due to their exchange cation deficiency. On the other hand, the preparation of ZSM5 catalytic coatings without the use of templates is highly desirable. When templates are used, they should be carefully removed; otherwise, part of the zeolite structure may collapse, making it difficult for the active cation to be exchanged.

The substrate of a structured catalyst can also influence the catalytic performance of the system [10]. For applications posing demanding conditions (vibrations, high flows and high temperature operations), metallic substrates present several advantageous properties such as higher mechanical resistance, thermal conductivity, thinner walls allowing higher cell densities, and lower pressure drop [11]. But the growth of zeolites on flat metal surfaces is difficult.

In direct synthesis, surface defects are needed for nucleation; in secondary synthesis, this roughness can also help in retaining the seeds. In the first case, physical treatments such as polished or acid leaching have been applied so as to develop roughness [12,13]; in the second case, a charge reversion procedure in which the surface is coated with a cationic polymer prior to seeding has been proposed [14].

An interesting metallic material for use as a support is a stainless steel (SS) FeCrAl thin foil that can secrete a superficial alumina film by high temperature treatments [15]. This could be useful for both direct or secondary synthesis of zeolites in which a homogeneous seeding could be obtained without the need for surface charge reversion.

Disordered crystalline ZSM5 coatings on SS 316 foils have been produced by direct synthesis with template to study the coverage and deposition efficiency on the support [16]. Likewise, a thin *b*-oriented silicalite coating has been obtained on SS 304 plates focusing on the effects of synthesis parameters [17]. One precedent can be found in the secondary synthesis of ZSM5 growths in various types of SS foils using polymer charge reversion and obtaining thin and *a*–*b* oriented films [12]. FeCrAl steel foils have recently been used for the in situ growth of disordered crystalline Ferrierite coatings [18].

The development of new structured catalysts having spatially oriented coatings on SS supports is of interest because both design aspects can play an important role in the catalytic performance of the system.

For all the above reasons, the present contribution presents the production of a continuous, ordered ZSM5 film onto an FeCrAl SS foil employing hydrothermal synthesis without the use of templates. The physicochemical and catalytic characteristics of the system are also analyzed. A structured monolith is tested in the catalytic selective reduction of NO_x with methane, previously exchanging indium in the zeolite framework as an active material. The relationship between the coating/system characteristics and the catalytic performance is finally discussed indicating its significance in the rational design of new structured catalysts.

2. Experimental

2.1. Materials

2.1.1. Support conditioning

Stainless steel (Goodfellow FeCrAl alloy (Fecralloy®)) foils of 50 μm thickness were calcined for 22 h at 900 °C in order to generate a surface layer of alumina. Before the hydrothermal synthesis, the pre-treated supports were subjected to a treatment in an ultrasonic bath with water for 15 min in order to remove contaminant particles and unstable oxide.

The growth characterizations were performed on strips of this material; a cylindrical monolithic structure was also built overlapping flat and corrugated strips. This monolith with sinusoidal channels was catalytically evaluated, its dimensions being 1.5 cm diameter × 3 cm long with a channel size of 1 mm. These dimensions were similar to those of a 400 cps washcoated cordierite monolith presented for comparison.

2.1.2. Hydrothermal synthesis conditions

The reactants employed were colloidal SiO_2 (Ludox® AS 40), $Na_2Al_2O_4$ (Riedel-de-Haen) and NaOH (Cicarelli pro-analysis) with proportions $H_2O{:}SiO_2{:}Na_2O{:}Al_2O_3 = 75{:}1.7{:}0.38{:}0.025$ that were modified with respect to the ratio used in a previous work [19], slightly increasing the silica content. This composition originated a theoretical Si/Al ratio of 34. Once the reactants were mixed, the gel was aged by stirring for 24 h at room temperature.

The hydrothermal treatment was performed for 24 h at 180 °C; both direct and secondary syntheses were employed in order to obtain the zeolitic growth. No template agents were used in the procedure.

2.2. Methods

2.2.1. Zeolite growth

The metallic supports were vertically fixed inside an autoclave together with the aged synthesis gel. Afterwards, they were placed in a stove at 180 °C for the hydrothermal treatment. In the case of secondary synthesis, prior to the introduction of the support, the gel was seeded with a 10 g/l nanocrystal suspension (200 nm) of NH_4-ZSM5 (Zeolyst; Si/Al = 15) according to a procedure previously described [19].

When the synthesis time was over, the autoclave was cooled and the samples were withdrawn, vigorously washed with a brush under water and afterwards treated in an ultrasonic bath for 10 min to remove residues from the solution. The remaining synthesis gel was filtered and the crystals produced were recovered. All the layer growths

and powder samples were finally dried in a stove at 120 °C for 4 h.

2.2.2. Monolith activation

In order to catalytically test the system, a ZSM5 coating was synthesized in a monolith. Once the Na-ZSM5/monolith was obtained, the activation was carried out through the incorporation of indium. An ammonium (80 °C, NO_3NH_4 1 M, 24 h) exchange was previously performed and after that, the indium impregnation was performed with an $In(NO_3)_3$ solution until obtaining a 4 wt.% indium loading with respect to the zeolite mass. The exchange of the indium species as compensation cations in zeolite was carried out by applying a thermal treatment at 500 °C in air flow for 12 h to generate the In_2O_3 oxides and decompose the ammonium in the zeolite. Then, the temperature was immediately increased to 700 °C during 2 h so as to develop the $(InO)^+$ sites by a solid-state reaction between impregnated In_2O_3 and zeolite protons [20].

2.3. Characterization techniques

2.3.1. X-ray diffraction (XRD)

Through this technique, it was possible to identify the crystalline phase of the crystals produced in the solution and in the growths obtained on the supports. A Shimadzu XD-D1 instrument operated at 40 kV and 30 A was employed with a scanning rate of 2° min^{-1} between $2\theta = 5°$ and 40° which is the range where the most important signals of the zeolite can be found. The diffraction patterns obtained were compared to those of pure ZSM5 powders, thus allowing the identification of the grown phase. On the other hand, the diffraction data were used to calculate crystallographic preferential orientations (CPO). The diffraction intensities of certain crystalline planes were compared to the intensities of the same planes in the zeolite powder. In this latter case, it is considered that the crystals are randomly oriented. The signals of the (200 + 020), (002) and (133) planes were related by the following expression [21]:

$$\mathrm{CPO}\frac{x}{y} = \frac{I^x_s/I^y_s - I^x_p/I^y_p}{I^x_s/I^y_s}$$

where I is the diffraction intensity from the planes with Miller's indexes x or y ($x = (002)$ or (133) planes; $y = (200 + 020)$ plane); s is the signals of the zeolite grown in the support; p is the signals of the zeolite powder.

2.3.2. Scanning electron microscopy (SEM)

This technique was used to determine the growth development on the support, its crystalline microstructure and the spatial ordering of the crystals. To do so, a SEM Jeol JSM-35C instrument was employed, operated at 20 kV acceleration voltages. The samples were glued to the sample holder with Ag painting and due to the low electrical conductivity of the zeolite, they were then coated with a thin layer of Au in order to improve the images.

2.3.3. Electron probe micro analysis (EPMA)

A dispersive EDAX instrument coupled to the SEM was employed to analyze the elemental composition of the growths. Several analyses were performed at different depths in the thickness so as to obtain the growth composition profile. This was achieved by scanning 1 μm wide areas of the coating thickness in a cross-section of the sample.

2.3.4. NO temperature-programmed desorption (NO TPD)

In order to characterize the indium species incorporated to the monolith, the interaction between the sample and a NO atmosphere was analyzed. The monolith was placed in a He flow at 400 °C in order to perform a surface cleaning; immediately after, it was put in contact with NO diluted in He (5000 ppm) for 20 min. Afterwards, the NO was purged from the gas phase and the temperature-programmed desorption was started at 10 °C min^{-1}, during which the IR spectra were acquired using a gas cell with CaF_2 windows.

2.3.5. Catalytic test in NO_x RCS with CH_4

The In-ZSM5/monolith was evaluated in a flow system emulating combustion effluents containing NO, CH_4 and O_2 in a He carrier. The experimental assembly details of the reactor can be found elsewhere [22]. The gas concentrations were 1000 ppm NO, 1000 ppm CH_4 and 10% O_2. The total flow was 71 cm^3/min, which in view of the zeolite mass present represents a F/W ratio of 500 cm^3/min gzeolite. This value is equivalent to a high space velocity and would correspond to a GHSV of 15,000 h^{-1} for the case of a zeolite powder with density = 0.5 g/cm^3. Since the density in the coating is much greater, the space velocity will be so in the same proportion.

The NO and methane conversions and the quantification of other gases such as CO were determined through the analysis of the reaction gases with an FTIR Thermo Mattson Genesis II instrument. This instrument was placed in line with the reactor and had a gas analysis cell. The gases measured were the CH_4, NO and NO_2 reactants and the CO, CO_2 and H_2O reaction products. Since N_2O was not detected, the difference between the amount of initial NO and the final $NO + NO_2$, is the N_2 produced by selective reduction.

The NO_x and CH_4 conversions and the NO to N_2 selectivity were calculated using the following equations, respectively:

$$X_{NO}(\%) = \frac{[NO]^0 - [NO + NO_2]_{final}}{[NO]^0} \times 100$$

$$X_{CH_4}(\%) = \frac{[CH_4]^0 - [CH_4]_{final}}{CH_4^0} \times 100$$

$$S_{NO} = \frac{X_{NO}[NO]^0}{X_{CH_4}[CH_4]^0}$$

3. Results and discussion

3.1. Growths obtained by direct synthesis

After subjecting the FeCrAl foils to the hydrothermal synthesis treatment under the said conditions (see Section 2), an XRD analysis of the sample was performed. The diffraction patterns showed the most important signals of ZSM5 and in certain cases weak signals of the Mordenite phase were also detected. Fig. 1a and b shows the XRD patterns obtained from the calcined steel foil and from the sample with the direct synthesis crystalline growth, respectively. In these experiments, a low weight increase due to the zeolite growth (about 1 wt.%) was in agreement with the weakness of the XRD signals. Fig. 1c shows the reference ZSM5 powder pattern for comparison.

On the other hand, the incipient Mordenite phase generated was more pronounced in the crystals recovered from the solution where a mixture of both zeolites was present, than on the support.

These results indicate that by direct synthesis under the stipulated conditions, the nucleation and growth path towards the ZSM5 phase over the support is preferred, even though its degree of development is very low. This is verified by SEM observations (Fig. 2a) that show a

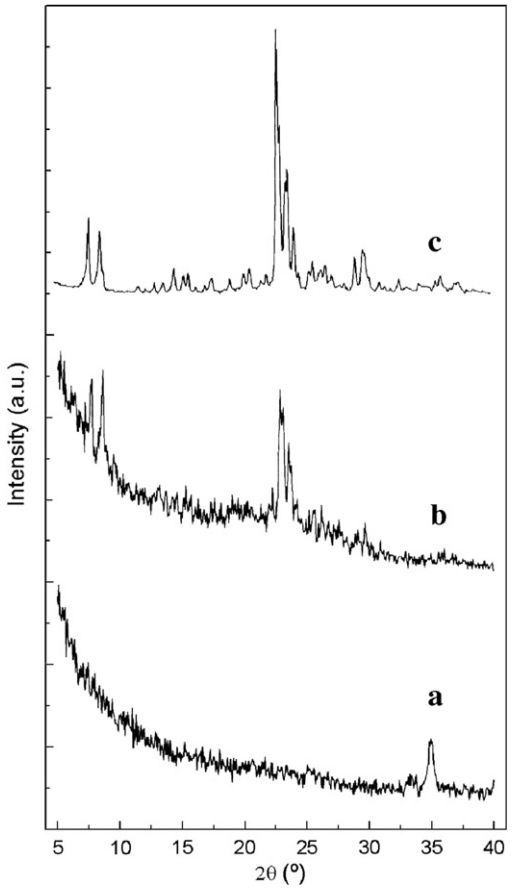

Fig. 1. XRD patterns obtained from: (a) calcined Fecralloy foil (4×); (b) calcined Fecralloy foil with the direct synthesis crystalline growth (4×) and (c) ZSM5 powder.

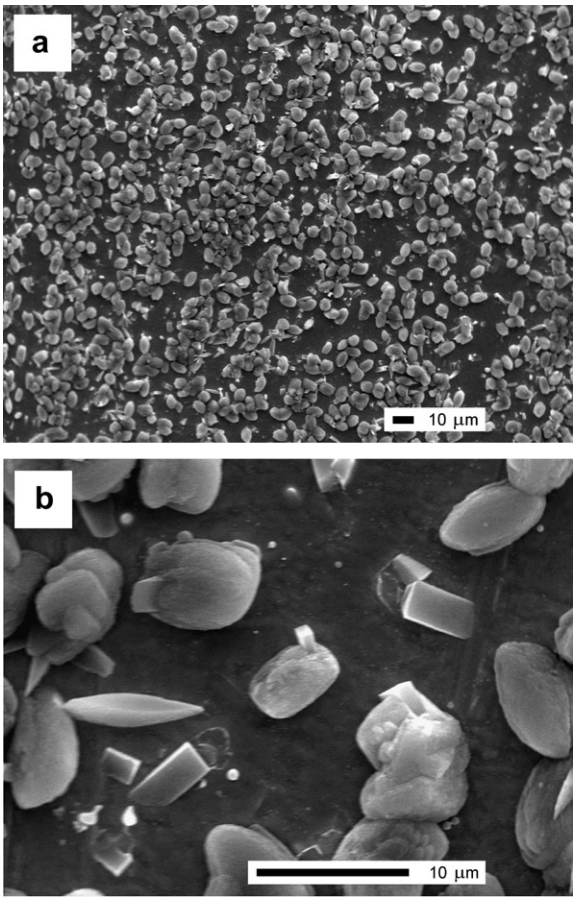

Fig. 2. SEM micrographs of the direct growth: (a) general view and (b) details of the crystals.

scarce development of crystals uniformly distributed on the support surface without totally covering it. Most crystals are 10μm long and present a rounded shape (Fig. 2b). This shape is proper to Al enriched ZSM5 crystals and is coherent with the fact that the support surface presented an alumina coating that was in contact with the zeolite nuclei during the crystalline growth. On the other hand, it is known that for the synthesis of ZSM5 crystals in solution when the Si/Al ratio of the gel is low, both nucleation and growth rates decrease noticeably [23]. Additionally, the number of nucleation sites on a support depends on their roughness because the germs start to grow in these superficial defects [13]. The low ZSM5 development achieved by direct synthesis on the support can be explained in terms of an insufficient superficial roughness and a small Si/Al ratio in the interphase during the synthesis. Both factors could contribute to the low zeolite nucleation and growth. Additionally, it should be remarked that this growth was obtained without employing any structuring agent and that this can also contribute to the low zeolite development.

3.2. Growths obtained by secondary synthesis

Given the reduced extension of the growth nucleation process over the FeCrAl support, this stage was decoupled

by means of a secondary hydrothermal synthesis. To achieve this, the support was previously seeded with ZSM5 nanocrystals and then subjected to hydrothermal treatment under the same conditions of direct synthesis.

After the hydrothermal treatment of the seeded support, two other consecutive treatments were performed without previous seeding. Fig. 3b–d presents the XRD patterns of the samples obtained with one to three hydrothermal syntheses. It can be observed that the growths are highly crystalline and exclusive of ZSM5.

The gel used was Si enriched compared to a previous one in which mordenite secondary growths were developed [19]. Using the composition of the previous gel, in this work we obtained a secondary growth made up of a mixture of mordenite and ZSM5 phases, which led to the modification of the said gel composition. Similar effects have been observed for synthesis in solution (powders) in which, with an increased Si content in the gel [24], a ZSM5 development was produced instead of mordenite.

In the samples with two and three syntheses, ZSM5 continued growing starting from the previous crystalline development. The XRD patterns (Fig. 3c–d) show that the ZSM5 phase was kept and the signal intensities increased, in accordance with a mass gain from 2.0, 3.5 and 8.6 wt.% for each treatment, respectively.

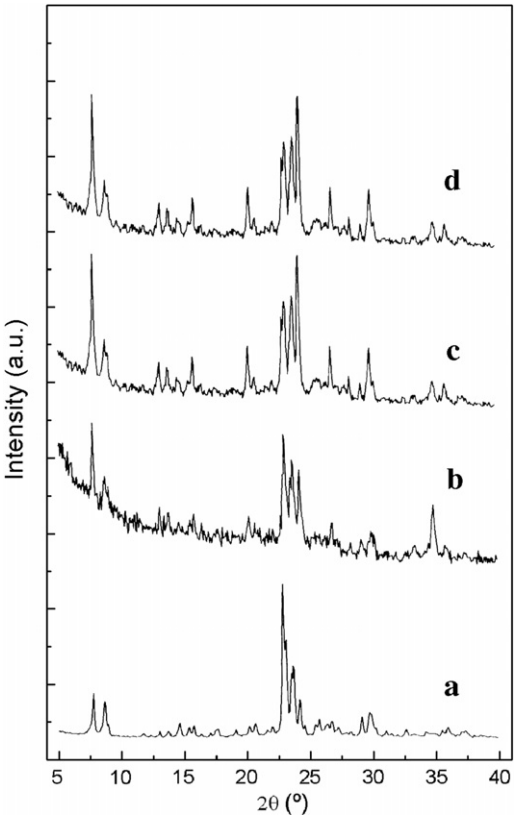

Fig. 3. XRD patterns of the secondary growths: (a) ZSM5 recovered powder (0.5×); (b) sample with only one hydrothermal synthesis; (c) sample with two hydrothermal syntheses and (d) sample with three hydrothermal syntheses.

The SEM observations of the sample with one synthesis (Fig. 4) confirm the presence of a dense crystalline growth totally covering the support, as can be observed in the top view of Fig. 4a. The intergrowth is high and the facet edges of the crystals overlap on the surface of the coating (1 μm edges), thus generating the characteristic topography. The side view (Fig. 4b) shows the high intergrowth of the coating exhibiting a columnar microstructure usually reported for MFI growths. The thickness was about 4.5 μm and it

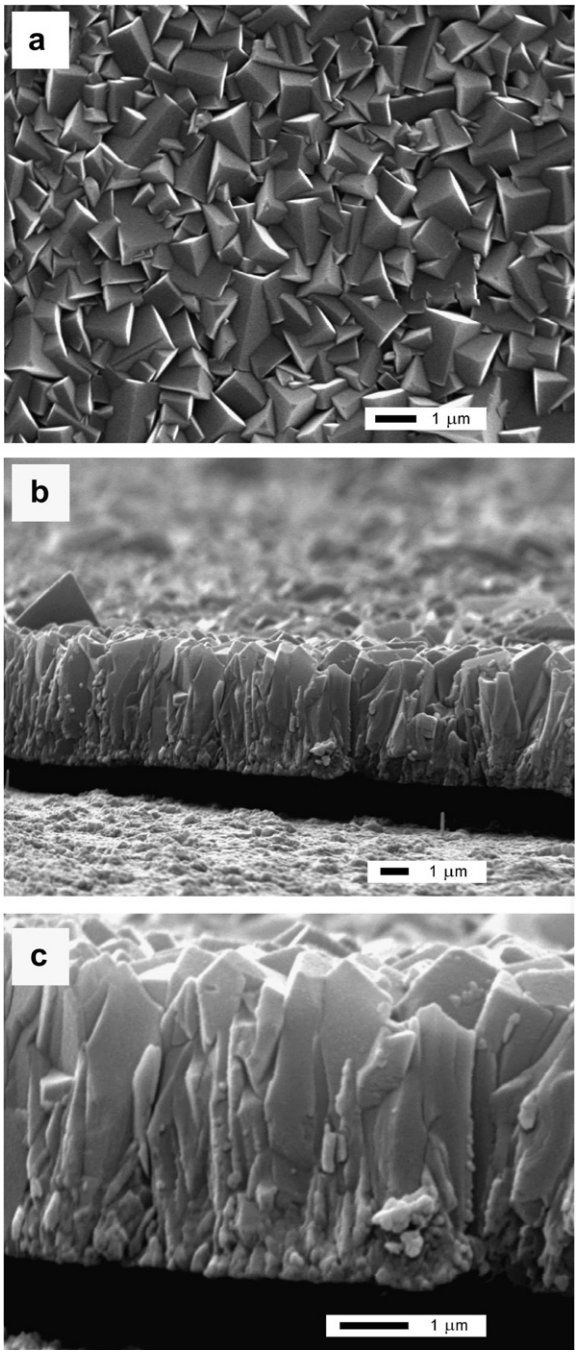

Fig. 4. SEM micrographs of the ZSM5 secondary growth obtained with one hydrothermal treatment (24 h): (a) top view; (b) side view and (c) close-up of the microstructure in the side view.

was highly adherent to the support (the separation between the coating and support is due to the SEM sample preparation). The details of the crystals can be noticed in the close-up view of Fig. 4c as well as the spatial disposition of the crystals with the tube-shaped geometry of the crystalline grains that start to grow from the original seeds.

The ZSM5 growth rate was high and around 180 nm h^{-1}, similar to the one presented by other ZSM5 growths on quartz substrates [25] and over α-alumina discs [26], which were obtained under similar hydrothermal conditions. The highest growth rates are produced when the crystallographic orientation proceeds in the *c*-direction, this direction being the one which grows faster.

The samples with 2 and 3 syntheses show similar structural characteristics than the 1 synthesis sample, but the size of the superficial facet edges of the crystals has increased having sides 3 μm long. In the micrograph of Fig. 5a the top view of the sample with 3 syntheses is displayed. This increasing grain size is consistent with the tube-shaped grain boundary morphology described above and is characteristic of the competitive growth mechanism proposed for this type of zeolite structure [6]. The transversal cross-section displayed in Fig. 5b shows a propagation of the edge lines of the crystal grains in the successive treatments but two slight discontinuities that interrupt these lines are noticed (see details in Fig. 5c). This coincides with the thicknesses produced after one and two syntheses, respectively, although hard ultrasonic treatments in water were performed between the growth steps. This discontinuity is also observed in the sample with two syntheses (not shown).

3.2.1. Crystallographic preferred orientation (CPO) of the secondary growths

In the diffraction patterns shown above (Fig 3b–d), it can be noticed that the signals present a modification of their relative intensities with respect to the powder signals (Fig. 3a). This indicates that in the growths, certain crystal planes are oriented. The spatial orientation of the planes is known as crystallographic preferred orientation and was confirmed in the SEM images previously shown, in which an important crystalline ordering can be seen.

Crystallographic orientations of silicalite growths [4] over silica wafers have been evaluated with a CPO $[(200+020)]/(133)$ ratio showing the orientation magnitude of the *a–b* crystallographic planes. On the other hand, the CPO $(002)/[(200+020)]$ ratio has been employed to evaluate ZSM5 orientations over quartz plates, showing the proportion of *c*-oriented planes [26].

The signals obtained from the ZSM5 powder produced in solution were taken as calculation reference (random orientation). Fig. 6 indicates the crystallographic planes of the signals considered for the calculation of CPO. When the CPO $(002)/[(200+020)]$ and $(133)/[(200+020)]$ present a value of 1 (maximum possible) they indicate that the crystals are perfectly oriented with the crystallographic *c*-axis perpendicular to the support or with an angle of 35°

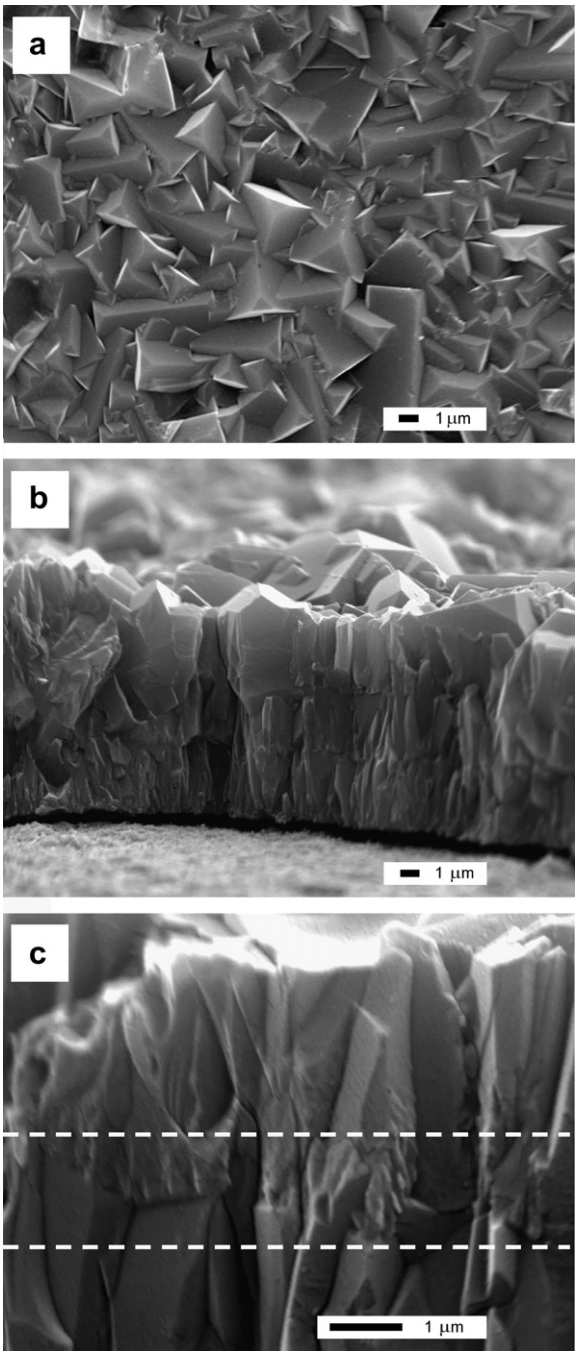

Fig. 5. SEM micrographs of the ZSM5 secondary growth obtained with three hydrothermal treatments: (a) top view; (b) cross-section and (c) close-up of the discontinuity in the side view (indicated between the lines).

with respect to the normal to the surface. Both situations are depicted in Fig. 7.

The CPO values obtained for the samples with 1, 2 and 3 syntheses are illustrated in Table 1. A great proportion of the crystals in the growth present an orientation of the *c*-axis perpendicular to the surface of the support. The proportion of crystals oriented with axis 133 is also high. According to these values, the 133 orientation could be slightly increased in the samples with two and three syntheses.

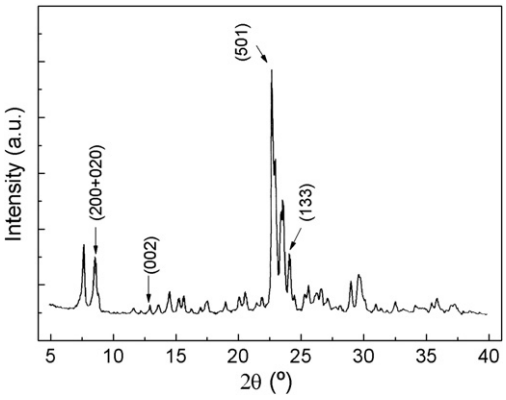

Fig. 6. Selected XRD signals in the XRD pattern of the ZSM5 for making CPO calculations. The reference pattern showed correspond to the ZSM5 crystals recovered from the solution gel after the synthesis.

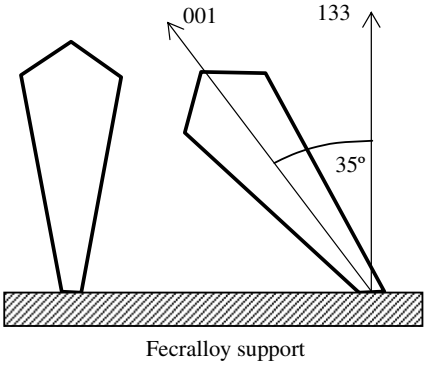

Fig. 7. Scheme of crystals grown with the 001-axis and the 133-axis perpendicular to support, respectively.

Table 1
CPO (002)/(200 + 020) and CPO (133)/(200 + 020) relations

Sample*	CPO(002)/(200 + 020)	CPO(133)/(200 + 020)
ZSM5[S1(2,0)]	0.79	0.40
ZSM5[S2(3,5)]	0.81	0.52
ZSM5[S3(8,6)]	0.78	0.67

* The number of syntheses and the zeolite weight increase (wt.%) are indicated between brackets.

The CPO values agree with the SEM observations presented before. Micrographs in Figs. 4 and 5 clearly show the position of the zeolite crystals with the longitudinal *c*-axis vertically oriented from the support.

3.2.2. Chemical composition of the secondary growths

The EPMA analyses were performed across the thickness of the coating in the growth achieved with three syntheses (see Section 2). The relative intensities of the signals in each sector analyzed were used to build the profile shown in Fig. 8. It can be noticed that Si, Al, Cr and Fe were detected and that the amount of silica increases towards the coating surface, thus indicating an aluminum enrichment in the sectors closer to the interphase. This

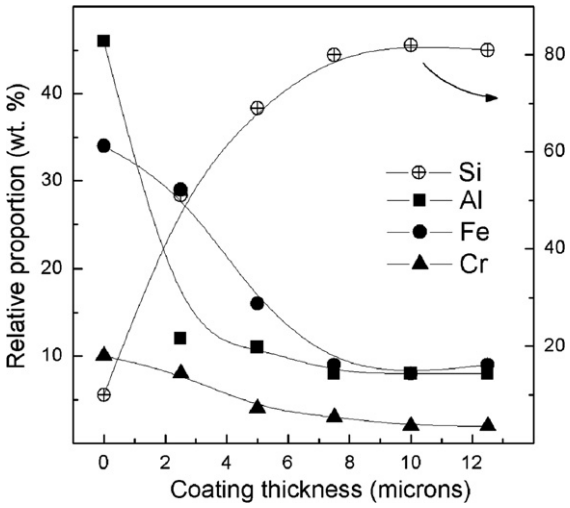

Fig. 8. EPMA profile performed on a transversal cross-section the ZSM5 growth obtained after three hydrothermal treatments. The analysis was performed at different depths in the coating.

could be due to a migration of the said element from the steel surface to the zeolite during the growth process. Simultaneously, the incorporation of Fe and Cr in the zeolite is produced, even though the type of species formed is unknown. Since no oxide signals were detected by XRD, they could be forming part of the zeolitic structure or else existing as small clusters of oxides dispersed in the intercrystalline spaces.

3.2.3. Zeolite layer stability in monoliths

The SEM pictures (Fig. 9) of a portion cut from the monolith wall after it was indium loaded and treated at 700 °C show that there is no apparent change in the structure of the ZSM5 growth and no coating detachment is observed, either. The sample was also subjected to ultra-

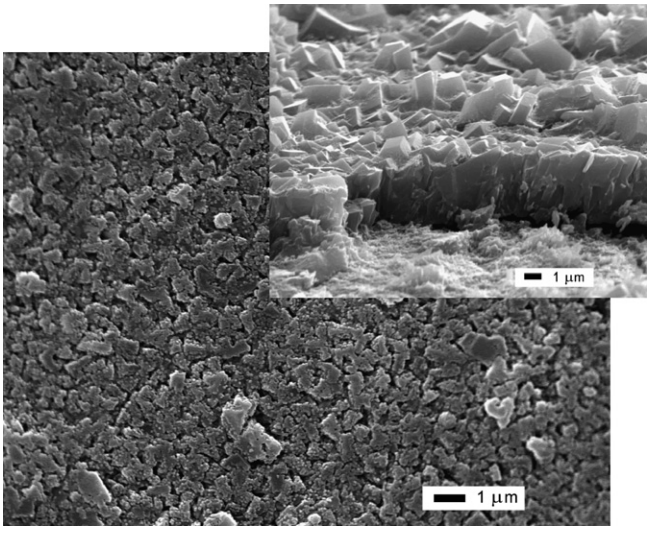

Fig. 9. SEM micrographs of the In-ZSM5/Fecralloy monolith surface after thermal activation at 700 °C.

sonic treatment in water for 30 min. The weight loss was negligible indicating a strong anchoring of the film.

On the other hand, small differences in the growth on the monolith walls are observed with respect to the growth on the sheets (Fig. 9). The grain boundaries among the crystals on the surface are a little less compact, and a secondary nucleation onto the first crystal growth is also observed. This indicates the coexistence of two mechanisms in the ZSM5 growth and has previously been reported [27]. In our work, the emergence of such secondary nucleation may be due to slight modifications in the seeding and/or growth conditions imposed by the confined environment of the channel geometry.

3.2.4. NO temperature-programmed desorption (NO-TPD) experiments

Fig. 10 presents the results of the NO-TPD test obtained for the monolithic sample with indium before the catalytic evaluation. For the sake of comparison, the desorption profile for an In-ZSM5 washcoated cordierite monolith is reproduced in the same figure [28]. Concerning the FeCrAl monolith, despite the fact that only NO was adsorbed, a desorption of NO_2 was observed in a single, sharp peak, close to 80 °C. The behavior of the washcoated In-ZSM5 sample is quite different; it presents one peak at about 80 °C and a wider desorption signal at higher temperature (centered around 300 °C). These different behaviors suggest that while in the case of the washcoated cordierite monolith different exchanged In species can exist, in the FeCrAl monolith there are In species exchanged in sites with a similar environment. It should be recalled that in indium-zeolite powder catalysts three indium species can exist [20]: highly dispersed oxides, bulk oxides, and InO^+ exchanged in the zeolite, the latter being the active species for the NO_x SCR. The NO_2 desorption in the samples (Fig. 10) is assigned to the presence of InO^+ species, which has oxygen available to oxidize the adsorbed NO into NO_2. On the other hand, the desorption of NO is considered to be produced on other indium species such as indium oxides. Thus, in the In-ZSM5/FeCrAl monolith the NO-TPD test suggests that In is present mainly in the form of exchanged InO^+ species, which is the active site for the NO_x SCR.

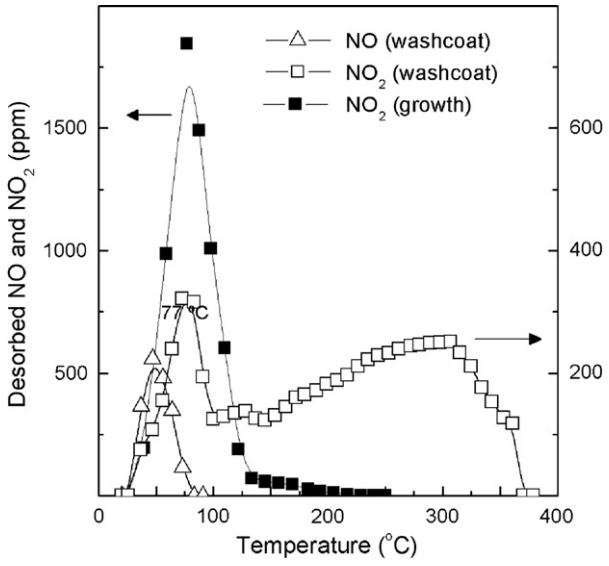

Fig. 10. NO-TPD characterization of the In-ZSM5/Fecralloy monolith. For comparison, the results for an In-ZSM5 washcoated monolith are included.

3.3. SCR of NO_x with CH_4. Evaluation of an In–ZSM5/FeCrAl monolith

Fig. 11a and b presents the catalytic behavior curves of this system. Fig. 11c and d shows the performance of an In–ZSM5 catalyst structured on a cordierite monolith by washcoating [22], which presents the same behavior as the powder catalyst. It should be remarked that the indium content and the evaluation conditions were the same in both cases (NO/CH_4 ratio; oxygen concentration and space velocity).

The In-ZSM5/FeCrAl catalyst presented a good NOx to N_2 conversion, the maximum reached being 74.5% against 86.0% of the catalyst used for comparison purposes (Fig. 10a–c). On the contrary, the selectivity was higher and in Fig. 10b–d it can be seen that the highest possible selectivity was reached at 450 °C.

A particular feature of this system was also the generation of CO as a reaction product. It can be observed that the amount produced by the In–ZSM5/FeCrAl system was lower than that of the reference catalyst, in the whole range of temperature (Fig. 10b–d). The decrease in the amount of CO can be attributed to the presence of oxidant iron species coming from the support and located in the coating as determined by EPMA. These species would be responsible for the oxidation of CO into CO_2. However, further research would be necessary to accurately know their location and nature.

The catalyst performance indicates that the efficiency of methane as NO_x reductant is maximum at 450 °C given the selectivity reached. That selectivity seems to be related to the low amount of non-selective indium species (the TPD indicated a single indium species, corresponding to InO^+ species) and to the generation of a smaller amount of CO.

The decrease in the NO_x conversion with respect to the washcoated powder cannot be attributed to differences in the nature of the active sites since the same exchange procedure was employed and the InO^+ species was present in both cases. An issue to be considered is the catalytic behavior of In-Mor/FeCrAl which was recently reported [19]. This catalyst exhibited a NO_x conversion higher to that of the powder (and washcoated) catalyst, attributed to a convenient crystallographic orientation of the mordenite film which facilitates the access of the reactants.

The characterizations performed in the present In–ZSM5/FeCrAl system suggest that the decrease in the NO_x conversion may be due to a diffusive restriction

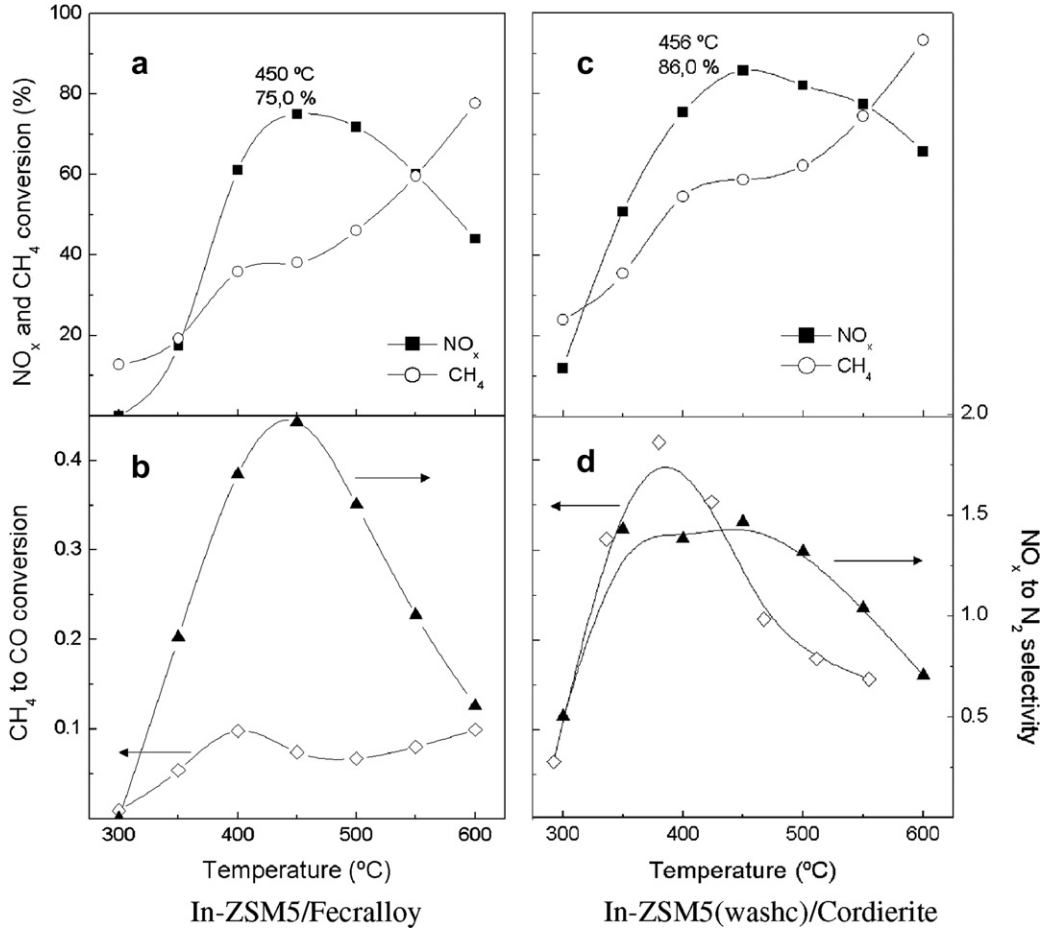

Fig. 11. Catalytic features of an In-ZSM5/stainless steel structured catalyst compared to those of In-ZSM5/cordierite catalyst obtained by washcoating (same features than the powder): (a and c) NO_x to N_2 and CH_4 conversion, respectively; (b and d) NO_x to N_2 selectivity and CO production, respectively.

caused by a disadvantageous situation of the spatial location of the crystals in the coating. The presence of a dense, intergrown coating was demonstrated, in which the crystals adopt a position with the *c*-axis perpendicular to the support. This situation implies that the zeolitic channels (which are in *a*- and *b*-directions) are parallel to the support surface. Since this zeolite has no channels in *c*, the entrance of reactants from the surface to the coating interior would be hindered if compared to a disordered location of the crystals as the one existing in the powder. Besides, the restriction to the reactants access posed by the orientation is imposed together with the high intergrowth, which limits the lateral access of the densely packed crystals.

4. Conclusions

Using secondary synthesis, an oriented ZSM5 structured catalyst is obtained grown on flat FeCrAl SS foils without employing templates. This catalyst presents a good performance in the SCR of NO_x with CH_4. The ZSM5 growth is a dense and thin film enriched with Al, Cr and Fe, with high intergrowth and an orientation of the zeolite crystals privileged with the *c*-direction perpendicular to the support.

The system has some advantages for its use as an environmental catalyst. The high mechanical resistance and thermal conductivity of the support allow its use under demanding conditions as in the SCR of NO_x application. The support needs no surface charge reversion to obtain a highly homogeneous coating thanks to the alumina segregated on the support. The catalytic coating has a high adherence, is active, produces less CO and presents a high selectivity, probably due to both the presence of Fe species in the coating and the fact that the main In species present are the InO^+ active species.

However, the system has an important disadvantage: the slight catalytic NO_x conversion decrease with respect to the powder. This could be attributed to the *c*-crystallographic axis orientation, perpendicular to the support. This fact implies a reduction in the zeolite channels available for the free diffusion of the reactants. In this way, the zeolitic channel spatial location with respect to the gaseous flux is disadvantageous leaving a lower accessibility to the active sites. The intergrowth emphasizes this aspect.

These results are also useful from the point of view of the design of structured catalysts. They show the impor-

tance of taking into account the coating structure characteristics and the chemical influence of the support for an optimum design of structured catalysts.

Acknowledgments

The authors wish to acknowledge the financial support received from CONICET, ANPCyT and Universidad Nacional del Litoral. Thanks are also given to Mario Montes from UPV, San Sebastián, Spain, for supplying the FeCrAl foils, to Fabio Fontanarrosa from Ceride-Conicet for the SEM-EPMA analysis, and to Elsa Grimaldi for the English language editing.

References

[1] P. Avila, M. Montes, E. Miró, Chem. Eng. J. 109 (2005) 11.
[2] A. Nijhuis, A. Beers, T. Vergunst, I. Hoek, F. Kapteijn, J. Moulijn, Catal. Rev. 43 (4) (2001) 345.
[3] J. Caro, M. Noack, P. Kolsch, R. Schafer, Micropor. Mesopor. Mater. 38 (2000) 3.
[4] J. Hedlund, S. Mintova, J. Sterte, Micropor. Mesopor. Mater. 28 (1999) 185.
[5] X. Zhang, H. Liu, K. Yeung, Mater. Chem. Phys. 96 (2006) 42.
[6] J. Hedlund, F. Jareman, Curr. Opin. Coll. Interface Sci. 10 (2005) 226.
[7] G. Bonilla, D. Vlachos, M. Tsapatsis, Micropor. Mesopor. Mater. 42 (2001) 191.
[8] A. Bons, P. Bons, Micropor. Mesopor. Mater. 62 (2003) 9.
[9] O. Ohrman, J. Hedlund, J. Sterte, Appl. Catal. A: Gen. 270 (2004) 193.
[10] J.M. Zamaro, M.A. Ulla, E.E. Miró, Appl. Catal. A: Gen. 314 (2006) 101.
[11] N. Burgos, M. Paulis, M. Montes, J. Mater. Chem. 13 (2003) 1458.
[12] Z. Wang, J. Hedlund, J. Sterte, Micropor. Mesopor. Mater. 52 (2002) 191.
[13] S. Mintova, V. Valtchev, L. Konstantinov, Zeolites 17 (1996) 462.
[14] S. Mintova, J. Hedlund, B. Schoeman, V. Valtchev, J. Sterte, Chem. Commun. 1 (1997) 15.
[15] J. Camra, E. Bielańska, A. Bernasik, K. Kowalski, M. Zimowska, A. Białas, M. Najbar, Catal. Today 105 (3–4) (2006) 629.
[16] Z. Shan, W. van Kooten, O. Oudshoorn, J. Jansen, H. van Bekkum, C. van den Bleek, H. Calis, Micropor. Mesopor. Mater. 34 (2000) 81.
[17] Z. Wang, Y. Yan, Micropor. Mesopor. Mater. 48 (2001) 229.
[18] E. Wloch, A. Lukaszczyk, Z. Zurek, B. Sulikowski, Catal. Today 114 (2006) 231.
[19] J.M. Zamaro, M.A. Ulla, E.E. Miró, Appl. Catal. A: Gen. 308 (2006) 161.
[20] E.E. Miró, L. Gutierrez, J.M. Ramallo López, F.G. Requejo, J. Catal. 188 (1999) 375.
[21] J.P. Verduijn, A.J. Bons, M.H. Anthonis, L.H. Czarnetzki, Int. Pat. Appl., PCT WO 96/01683.
[22] J.M. Zamaro, M.A. Ulla, E.E. Miró, Chem. Eng. J. 106 (2005) 25.
[23] A.E. Persson, B.J. Schoeman, J. Sterte, J.E. Otterstedt, Zeolites 15 (1995) 611.
[24] H. Lechert, Micropor. Mesopor. Mater. 40 (2000) 181.
[25] S. Mintova, J. Hedlund, V. Valtchev, B. Schoeman, J. Sterte, J. Mater. Chem. 8 (10) (1998) 2217.
[26] J. Hedlund, M. Noack, P. Kolsch, D. Creaser, J. Caro, J. Sterte, J. Membr. Sci. 159 (1999) 263.
[27] M. Vilaseca, E. Mateo, L. Palacio, P. Prádanos, A. Hernández, A. Paniagua, J. Coronas, J. Santamará, Micropor. Mesopor. Mater. 71 (2004) 33.
[28] J.M. Zamaro, Ph.D. Thesis, Facultad de Ingeniería Química (UNL) 2005.